Chemistry–A European Journal
Research Article
doi.org/10.1002/chem.202303696
Chemistry Europe
European Chemical Societies Publishing
www.chemeurj.org

Hot Paper

The Phosphidosilicates $AE_2Li_4SiP_4$ (AE = Ca, Sr, Eu) $Ba_4Li_{16}Si_3P_{12}$

Martin L. Weidemann,[a] Robert Calaminus,[a, b] Nina Menzel,[a] and Dirk Johrendt*[a]

The quaternary phosphidosilicates $AE_2Li_4SiP_4$ (AE = Ca, Sr, Eu) and $Ba_4Li_{16}Si_3P_{12}$ were synthesized by heating the elements and Li_3P under argon atmosphere. Their crystal structures were determined by single crystal X-ray diffraction. $AE_2Li_4SiP_4$ crystallize in a new layered structure type ($P2_1/m$, Z = 2) with CdI_2-analoguos layers. Edge sharing CaP_6 octahedra are separated by layers of vertex-sharing SiP_4 and LiP_4 tetrahedra, which contain additional chains of LiP_6 octahedra. $Ba_4Li_{16}Si_3P_{12}$ forms likewise a new structure type ($P2_1/c$, Z = 16) with a three-dimensional network of SiP_4, Si_2P_6 and LiP_4 entities as well as one phosphorus site not bonded to silicon. Barium is located in capped trigonal prisms of phosphorus which form strongly corrugated layers. ^{31}P and ^{29}Si solid-state NMR spectra confirm the crystal structures of the compounds $AE_2Li_4SiP_4$. ^{7}Li spectra show only one signal in spite of quite different crystallographic positions, which indicate possible Li^+ mobility. However, this signal is much broader compared to the known Li^+ conducting phosphidosilicates. Accordingly, electrochemical impedance measurements show low Li^+ conductivities.

Introduction

Phosphidosilicates consist of SiP_4 tetrahedra which occur isolated or linked to form oligomers, chains, or networks. They are thus related to oxido- and nitridosilicates, but their structural versability is even greater due to their ability to form P–P and Si–Si bonds. Alkaline and alkaline earth phosphidosilicates have been known since the end of the 20th century, however, potential applications in optics or energy storage are currently leading to a growing interest in these compounds. The highly charged tetrahedral ortho-anion $[SiP_4]^{8-}$ occurs exemplarily in AE_4SiP_4 (AE = Ca, Sr, Ba),[1] Li_8SiP_4,[2] and $Li_{14}SiP_6$.[3] $Li_{10}Si_2P_6$[4] and $Na_{10}Si_2P_6$[5] contain $[Si_2P_6]^{10-}$ dimers of edge sharing tetrahedra. Surprisingly, Cs_5SiP_3 forms no tetrahedra but unique trigonal-planar $[SiP_3]^{5-}$-anions.[6] More common are compounds with higher degrees of condensation. Examples are vertex or edge condensed chains in A_2SiP_2 (A = Na, K, Cs),[7–9] $Ba_4Si_3P_8$[10] or $Ba_2Si_3P_6$.[11] Further condensation leads to supertetrahedra denominated as Tn (n = 2 –5), where n is the number of base tetrahedra along the edges of the supertetrahedra.[12] $Ca_2Si_2P_4$[13] and the low temperature modification of KSi_2P_3[14] consist of T2 or T3 entities forming layered structures. In contrast, Li_2SiP_2[15] and $AESi_7P_{10}$ (AE = Sr, Ba) form three dimensional networks derived from T2 clusters. Larger supertetrahedral structures up to T5 exist in $LiSi_2P_3$,[15] the high temperature modification of KSi_2P_3,[16] and in $Na_{23}Si_{9n+19}P_{12n+33}$ (n = 0-3).[17] Many phosphidosilicates contain P–P bonds,[4,10,13,18–20] while such homonuclear bonds between the anions do not occur in nitrido- and oxidosilicates. The cations are not limited to main group elements. By elaborate synthetic techniques such as flux or transport agents to prevent the formation of stable binaries,[21–23] rare-earth metals can be used as well, often yielding in phosphosilicides.[24–28] In the last years, a number of phosphidosilicates have proven to be good ion conductors. Examples are the Li^+ conductors Li_8SiP_4,[2] $Li_{14}SiP_6$[3] and $LiSi_2P_3$,[15] Na^+ ion conductors $Na_{19}Si_{13}P_{25}$ and the series $Na_{23}Si_{9n+19}P_{12n+33}$,[17] as well as the K^+ ion conductor KSi_2P_3.[16] In light of these findings, we have been searching for new quaternary lithium phosphidosilicates that may also have potential ion-conducting properties. We encountered the new compounds $Ca_2Li_4SiP_4$, $Sr_2Li_4SiP_4$, $Eu_2Li_4SiP_4$, and $Ba_4Li_{16}Si_3P_{12}$ with previously unknown structure types. Here we report the synthesis, crystal structures, and solid-state NMR characterization of these four quaternary phosphidosilicates.

Results and Discussion

The title compounds were synthesized by solid-state reactions of stoichiometric mixtures of the elements under argon atmosphere using self-prepared Li_3P as lithium source. Two-step reactions with identical temperature programs resulted in polycrystalline products, which rapidly decompose in air to unknown products. All crystal structures were solved from single-crystal diffraction datasets using direct methods[29] and refined in the space groups $P2_1/m$ for $AE_2Li_4SiP_4$ and $P2_1/c$ for $Ba_4Li_{16}Si_3P_{12}$. Basic crystallographic data are compiled in Table 1, fractional atomic positions, equivalent and anisotropic displace-

[a] M. L. Weidemann, R. Calaminus, N. Menzel, Prof. Dr. D. Johrendt
Department Chemie
Ludwig-Maximilians-Universität München
Butenandtstrasse 5–13(D), 81377 München (Germany)
E-mail: johrendt@lmu.de
[b] R. Calaminus
Max-Planck-Institut für Festkörperforschung
Heisenbergstr. 1, D-70569 Stuttgart

Supporting information for this article is available on the WWW under https://doi.org/10.1002/chem.202303696

Table 1. Crystallographic data on the single-crystal structure solution and refinement of $AE_2Li_4SiP_4$ (AE = Ca, Sr, Eu) and $Ba_4Li_{16}Si_3P_{12}$.

Compound	$Ca_2Li_4SiP_4$	$Sr_2Li_4SiP_4$	$Eu_2Li_4SiP_4$	$Ba_4Li_{16}Si_3P_{12}$
space group	$P2_1/m$ (no. 11)	$P2_1/m$ (no. 11)	$P2_1/m$ (no. 11)	$P2_1/c$ (no. 14)
a/Å	6.7229(8)	6.9972(1)	6.9016(2)	16.6933(3)
b/Å	8.2100(9)	8.3779(1)	8.3330(2)	11.5994(2)
c/Å	7.1669(8)	7.3171(1)	7.2403(2)	29.5092(6)
β/°	90.064(4)	90.105(1)	90.1190(10)	115.2770(10)
V_{cell}/Å^3	395.58(8)	428.941(10)	416.396(19)	5166.85(17)
Z	2	2	2	8
$\rho_{X\text{-ray}}$/g cm^{-1}	2.182	2.748	3.857	2.870
μ/mm^{-1}	2.295	13.223	15.735	6.888
Θ-range/°	2.842 - 30.633	2.784 - 36.394	2.813 - 30.564	2.146 - 36.390
refl. measured	10240	16009	14333	244409
independent refl.	1290	2165	1344	25091
parameters	61	61	61	643
R_σ	0.0252	0.0153	0.0246	0.0202
R_{int}	0.0389	0.0224	0.0478	0.0384
R_1 ($F^2 > 2\sigma$ (F^2))/all	0.0250/0.0324	0.0136/0.0159	0.0167/ 0.0179	0.0385/0.0468
wR_2 ($F^2 > 2\sigma$ (F^2))/all	0.0566/0.0588	0.0523/0.0530	0.0408/ 0.0413	0.0734/0.0760
GooF	1.107	1.375	1.087	1.245
$\Delta\rho_{max/min}$/e Å^{-3}	+0.409/−0.641	+0.527/−0.593	0.798/−1.875	+3.903/−1.776
restraints	0	0	0	1

ment factors are given in the Tables S1-S8 in the Supporting Information. Deposition Numbers CSD-2303649 ($Ca_2Li_4SiP_4$), CSD-2303650 ($Sr_2Li_4SiP_4$), CSD-2303651 ($Eu_2Li_4SiP_4$), and CSD-2303652 ($Ba_4Li_{16}Si_3P_{12}$) contain the supplementary crystallographic data for this paper. These data are provided free of charge by the joint Cambridge Crystallographic Data Centre and Fachinformationszentrum Karlsruhe Access Structures service. Rietveld refinements calculated using the single crystal data as initial parameters show that all samples contain less than 5% impurities (Figure 1).

$Ca_2Li_4SiP_4$ forms a new layered structure type which can be described as a filled variant of the hexagonal CdI_2-type (Figure 2). Phosphorus forms a distorted hexagonal packing (hp) with calcium atoms in one half of the octahedral voids (o), so that every second closed packed layer is filled. Lithium atoms are in 1/4 of the remaining octahedral voids as well as in 3/8 of the tetrahedral holes (t) between the CaP_2-layers. Silicon atoms occupy 1/8 of the tetrahedral voids between the CaP_2-layers. With this one can write the formula as $(Ca^o)_2(Li^t)_3(Li^o)Si^t(P^{hp})_4$. Figure 3 shows the linkage pattern of the SiP_4 and LiP_4 tetrahedra. The octahedrally coordinated lithium atoms form chains running along the b-direction. Attempts to synthesize $Ba_2Li_4SiP_4$ were unsuccessful, and instead we discovered the lithium richer compound $Ba_4Li_{16}Si_3P_{12}$. Its crystal structure is more complex ($P2_1/c$, Z = 8), and it is not an ortho-phosphidosilicate despite the matching composition. In addition to isolated $[SiP_4]^{8-}$ tetrahedra, $[Si_2P_6]^{10-}$ groups and phosphide ions (P^{3-}) not bonded to silicon are now present, which are required for charge balance according to the ion formula $Ba^{2+}{}_8Li^+{}_{32}[SiP_4]^{8-}{}_5[SiP_3]^{5-}P^{3-}$. Figure 4 emphasizes the three-dimensional network of SiP_4, Si_2P_6 and LiP_4 entities with barium atoms in channels along the a-axis. The Si–P bond lengths of 2.25 Å to 2.42 Å are in the range typical for phosphidosilicates, while the Li–P distances cover a relatively wide range. The LiP_4 tetrahedra in Figure 4 include distances from 2.43 Å up to 3.0 Å, while 3 out of the 33 crystallographically different lithium positions do not reach fourfold coordination up to this distance. This wide distribution of the bond lengths and the partially less symmetric environments may indicate mobility of the lithium ions. The barium atoms are located in channels along [100] and form strongly corrugated layers of capped trigonal BaP_7 prisms by considering Ba–P distances up to 3.8 Å (Figure 4, bottom). One exception is the Ba5 position, which has six relatively short bonds (3.20–3.36 Å) forming the BaP_6 prism capped by a phosphorus atom at 3.91 Å distance. Figure 5 shows details of the $[Si_2P_6]^{10-}$ unit and of the phosphide ion site which is not bonded to silicon. The latter is coordinated by seven lithium and two barium atoms, forming a threefold capped trigonal prism. Such a PM_9 coordination is typical and occurs in many metal phosphides.

NMR measurements under MAS conditions were performed for ^{7}Li, ^{29}Si and ^{31}P nuclei in $Ca_2Li_4SiP_4$ and $Sr_2Li_4SiP_4$. The patterns of the ^{31}P- and ^{29}Si-spectra (Figure 6) are consistent with the number of crystallographic atom positions, respectively. The phosphorus nuclei show three distinct resonance frequencies at $\delta(^{31}P)$ = −101.4, −113.0, −185.8 ppm for $Ca_2Li_4SiP_4$ and $\delta(^{31}P)$ = −145.2, −160.4, −210.7 ppm for $Sr_2Li_4SiP_4$, indicating three magnetically inequivalent

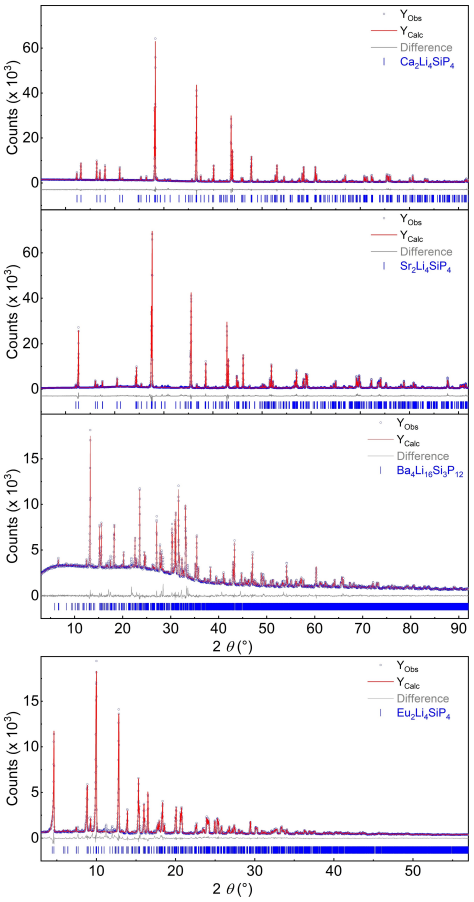

Figure 1. X-ray powder diffraction patterns (Y_{Obs}, blue), Rietveld fits (Y_{Calc}, red), and difference lines (gray) of $Ca_2Li_4SiP_4$, $Sr_2Li_4SiP_4$ and $Ba_4Li_{16}Si_3P_{12}$ measured with Cu–Kα1 radiation, and $Eu_2Li_4SiP_4$ measured with Ag–$Kα_1$ radiation.

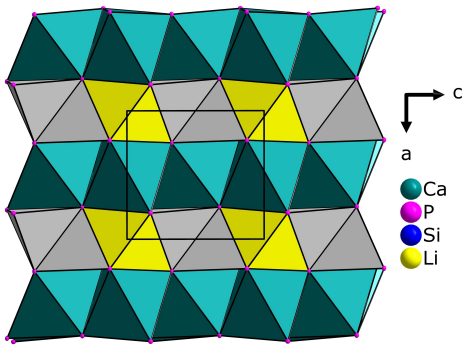

Figure 2. Crystal structure of $Ca_2Li_4SiP_4$ projected in [010] with CaP_6-octahedra (green), LiP_4-tetrahedra (yellow) and LiP_6-octahedra (grey).

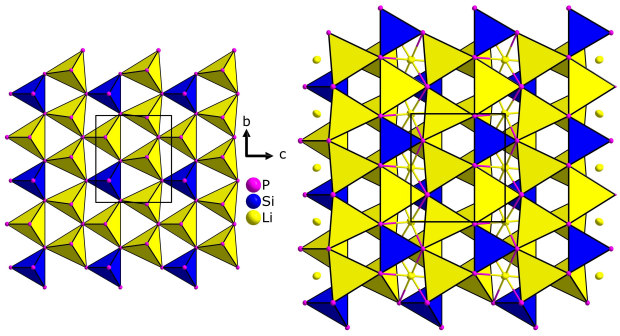

Figure 3. Left: Layer of vertex sharing LiP_4- (blue) and SiP_4-tetrahedra (yellow) in $AE_2Li_4SiP_4$ (AE = Ca, Sr, Eu). Right: With crystallographically equivalent second layer and intervening Li atoms in octahedral coordination.

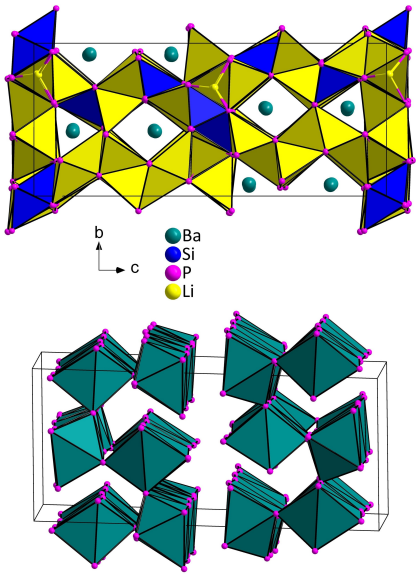

Figure 4. Crystal structure of $Ba_4Li_{16}Si_3P_{12}$. Top: Network of SiP_4, Si_2P_6 (blue) and LiP_4 (yellow) entities viewed along the *a*-axis. Lithium atoms with three phosphorus neighbours are shown without polyhedra. Bottom: Strongly corrugated layers of BaP_7 single-capped trigonal prisms in the ab-plane.

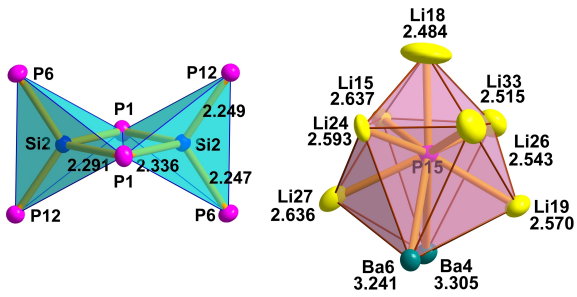

Figure 5. Details of the crystal structure of $Ba_4Li_{16}Si_3P_{12}$. Edge-sharing tetrahedra in the Si_2P_6 units (left) and coordination of the P15-atom by seven lithium and two barium cations forming a tricapped trigonal prism (right).

phosphorus atoms with differing intensities referring to the Wyckoff positions 2×2*e* and 4*f*. The distinction of possible *J* couplings is not possible here due to the linewidths of the ^{31}P NMR resonances (fwhm ≈500 Hz). The wide range of the spinning sidebands of the ^{31}P spectrum (~200 ppm) indicates a fairly large anisotropy of the chemical shift tensor in accordance with other Li-rich phosphidosilicates.[4] In the Si-spectra a single resonance frequency each in $\delta(^{29}Si) = -3.1$ ppm for $Ca_2Li_4SiP_4$ and $\delta(^{29}Si) = -9.1$ ppm for $Sr_2Li_4SiP_4$ is consistent to one silicon site. The well-resolved signal of $Sr_2Li_4SiP_4$ splits up due to coupling with the four surrounding phosphorus atoms. The ^{7}Li-spectra exhibit one signal at $\delta(^{7}Li) = 2.9$ ppm for $Ca_2Li_4SiP_4$ and $\delta(^{7}Li) = 3.2$ ppm for $Sr_2Li_4SiP_4$ contradicting the three Li-posi-

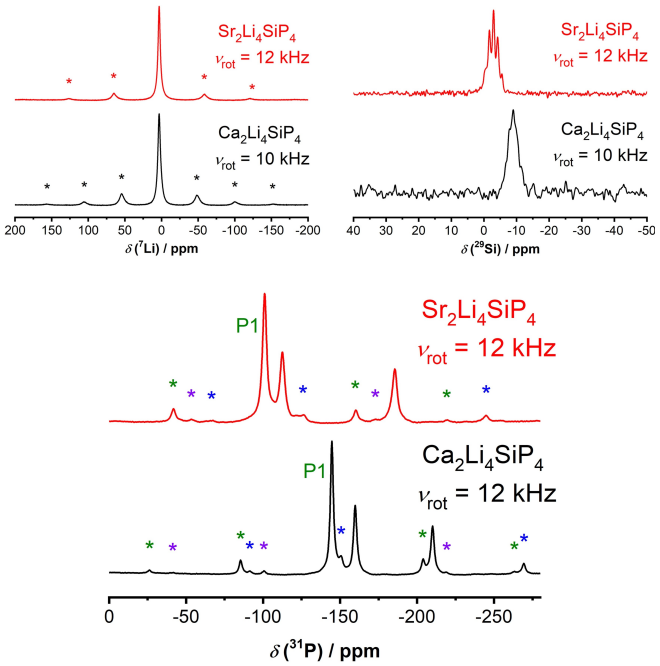

Figure 6. MAS-NMR spectra of ^{7}Li (top, left), ^{29}Si (top, right) and ^{31}P (bottom) at 10 kHz of $Ca_2Li_4SiP_4$ and $Sr_2Li_4SiP_4$. Rotation side bands marked with stars. Respective chemical shifts are δ (^{7}Li,) = 2.9 ppm, δ (^{29}Si) = −3.1 ppm and δ (^{31}P) = −101.4, −113.0, −185.8 ppm for $Ca_2Li_4SiP_4$ and δ (^{7}Li,) = 3.2 ppm, δ (^{29}Si) = −9.1 ppm and δ (^{31}P) = −145.2, −160.4, −210.7 ppm for $Sr_2Li_4SiP_4$.

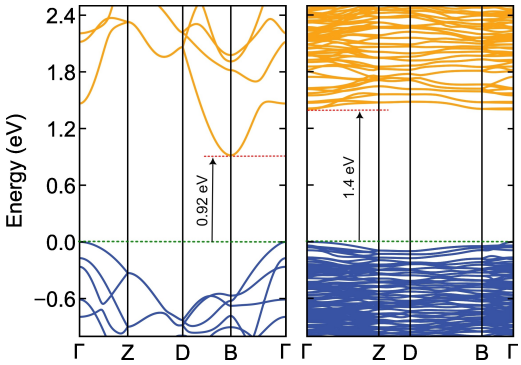

Figure 7. Cutouts of the electron band structures of $Ca_2Li_4SiP_4$ (left) and $Ba_4Li_{16}Li_3P_{12}$ (right).

tions. However, the relatively broad signal may be a superposition of three signals at very similar chemical shifts. This broad signal indicates that the ions are less mobile than in known Li-ion conducting phosphidosilicates, in which the ^{7}Li signals are narrower by one order of magnitude.[15]

DFT calculations of the electron band structures using VASP with PBE potentials reveal similar indirect band gaps for $AE_2Li_4SiP_4$ (*AE* = Ca: 0.92 eV, Sr: 1.08 eV, Eu: 0.94 eV) and a significantly bigger direct gap of 1.4 eV for $Ba_4Li_{16}Si_3P_{12}$. Calculations using meta-GGA approaches increase the gaps by 0.5-0.7 eV. Due to the orange color of $Ca_2Li_4SiP_4$ and $Sr_2Li_4SiP_4$, their band gaps should be above 2 eV. However, DFT methods are known to often underestimate band gaps. Our samples of $Ba_4Li_{16}Si_3P_{12}$ are black due to the presence of unidentified impurities, $Eu_2Li_4SiP_4$ is likewise black. The bands and density of states diagrams (Figures S4–S8) reveal that the *d*-orbitals of the alkaline earth atoms mainly contribute to the bottom of the conduction bands. The smaller bandgaps of the $AE_2Li_4SiP_4$ compounds are due to one single band whose energy becomes lower at the B point (Figure 7, left). Without this, the band gaps of the $AE_2Li_4SiP_4$ compounds would be bigger and similar to that in $Ba_4Li_{16}Si_3P_{12}$, where this lowered band is not present (Figure 7 right). Calculations of the phonon dispersions (Figures S6, S9) show no imaginary modes, which proves the mechanical stability of the compounds.

Electric properties of the compounds were investigated using electrochemical impedance spectroscopy (EIS, Figure 8) and chronopotentiometry (Figures S10–S12). $Ca_2Li_4SiP_4$ shows a polarization tail, $Sr_2Li_4SiP_4$ and $Eu_2Li_4SiP_4$ do not. The absence of a clear polarization tail in the EIS spectra suggests that those compounds are mixed ion-electron conductors (MIEC). A description of the equivalent circuits used for fitting is given in the SI. The EIS of $Ca_2Li_4SiP_4$ (Figure 8, top) results in a total ionic conduction of 6.8×10^{-9} S/cm describing the combined ionic processes in the sample. This is in acceptable agreement with the values obtained by Chronopotentiometry (Figure S10) of 4.0×10^{-9} S/cm for the ionic, 7.7×10^{-10} S/cm for the electronic and 4.8×10^{-9} S/cm for the total electric conductivity, which defines the entirety of conduction effects present in the sample. The activation energy was calculated to be 0.416(2) eV using the Arrhenius equation with the total ionic conductivity derived by EIS. The transference number was calculated to be $t_{ion} = 0.90$. Unlike $Ca_2Li_4SiP_4$, $Sr_2Li_4SiP_4$ (Figure 8, middle) does not appear to have a polarization tail, but shows rather the beginning of another semicircle. Fitting the impedance data yields an ionic conductivity of 1.7×10^{-7} S/cm and an electronic conductivity of 8.3×10^{-9} S/cm at room temperature, resulting in a total electric conductivity of 1.8×10^{-7} S/cm. The value of the electronic conductivity is in good agreement with the one obtained by chronopotentiometry (Figure S11) of 8.0×10^{-9} S/cm. However, the total electric conductivity and the ionic conductivity calculated from chronopotentiometry are around one order of magnitude lower, which could indicate a decay of the sample over time ($\sigma_{ion} = 2.5\times10^{-8}$ S/cm, $\sigma_{total} = 3.1\times10^{-8}$ S/cm). The ionic transference number t_{ion} is 0.95 if calculated from EIS and 0.81 if calculated from chronopotentiometry. The activation energy of the ionic process is 0.27(2) eV and the activation energy of the electronic process is 0.50(2) eV. The EIS of $Eu_2Li_4SiP_4$ (Figure 8, bottom) shows a total electric conductivity of 1.1×10^{-4} S/cm and does not allow for distinguishing between ionic and electronic conduction. The activation energy is determined as 0.057(1) eV. The presence of a semi-circle within the EIS spectrum, however, implies the occurrence of a capacitive process. Chronopotentiometry at room temperature yields an electronic conductivity of 1.3×10^{-4} S/cm and a total electric conductivity of 1.3×10^{-4} S/cm (Figure S12), which is in good agreement with the conductivity from EIS. The ionic conduction, if present, would therefore have to be several orders of magnitude smaller than the electronic conductivity. To evaluate the presence of ionic transport, the sample was measured in an

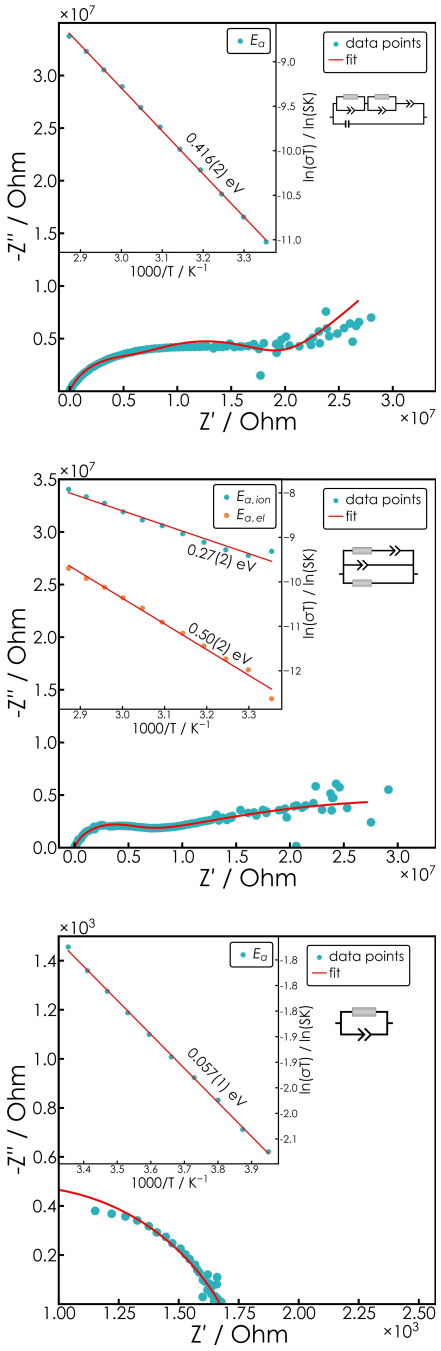

Figure 8. Room temperature electrochemical impedance spectra of $Ca_2Li_4SiP_4$ (top), $Sr_2Li_4SiP_4$ (middle) and $Eu_2Li_4SiP_4$ (bottom). Temperature-dependent Arrhenius plots as well as the equivalent circuits are given as insets.

electron-blocking configuration, resulting in no meaningful data. It is therefore concluded that $Eu_2Li_4SiP_4$ has no noteworthy ionic conductivity.

Conclusions

The ortho-phosphidosilicates $AE_2Li_4SiP_4$ (EA = Ca, Sr, Eu) crystallize in a new structure type related to the CdI_2 type structure with silicon and lithium atoms ordered in the voids between layers of CaP_6 octahedra. $Ba_4Li_{16}Si_3P_{12}$ is a lithium richer phosphidosilicate-phosphide which contains LiP_4 entities as well as one phosphorus site not bonded to silicon. Barium is located in channels of the network and sevenfold coordinated by phosphorus. Evidently, the barium atoms are too large for the octahedral voids of a hexagonal packing of phosphorus atoms as present in the $AE_2Li_4SiP_4$ compounds, which gives way to this more complex structure. ^{31}P and ^{29}Si NMR results agree with the crystal structure and ^{7}Li-spectra indicate rather low Li^+ ion mobility. Accordingly, electrical impedance measurements exhibited low Li^+ ion conductivities for $Ca_2Li_4SiP_4$ (6.8×10^{-9} S/cm) and $Sr_2Li_4SiP_4$ (1.7×10^{-7} S/cm), which are three to four orders of magnitude below the Li^+ conductivities of known ternary lithium-phosphidosilicates like $Li_{14}SiP_6$ (10^{-3} S/cm)[3] and $LiSi_2P_3$ (2×10^{-4} S/cm).[15] The title compounds also feature electrical conductivity at nearly the same order of magnitude. Therefore, these phosphidosilicates can be viewed as mixed conductors. In contrast $Eu_2Li_4SiP_4$ shows no significant ion conductivity but much higher electronic conductivity.

Experimental Section

Synthesis

$Ca_2Li_4SiP_4$, $Sr_2Li_4SiP_4$, $Eu_2Li_4SiP_4$ and $Ba_4Li_{16}Si_3P_{12}$ were prepared by heating stoichiometric amounts of Ca metal (99%, Merck), Sr metal (99.95%, SMT Metalle Wimmer), Eu metal (99.95%, SMT Metalle Wimmer), Ba metal (99.99%, Sigma Aldrich), Si powder (99,99%, AlphaAesar), P (99.999%, chempur) and self-prepared Li_3P. The reaction mixtures were filled in alumina crucibles and welded in silica tubes under purified argon atmospheres. Reactions were carried out at 900 °C for 48 h with heating of 20 °C/h. In a second step the samples were cooled down with 10 °C/h to 500 °C to enhance crystal growth and then with 200 °C/h to room temperature. Repeating the same temperature program twice after respectively pressing a pellet (1 t) yielded air-sensitive polycrystalline powders.

Single-Crystal X-ray Diffraction

Crystals of sufficient quality were selected under dried paraffin oil and transferred into oil-filled glass capillaries (Hilgenberg GmbH, Malsfeld, Germany, inner diameter 0.2 mm). Diffraction data were collected using a Bruker D8 Quest diffractometer (Mo–Kα X-ray source, Göbel mirror optics, Photon II CPAD detector). For data reduction and absorption correction the software package APEX3[30] was used. Space group determination was carried out with XPREP[31] based on systematically absent reflections. OLEX2[32] was used for structure solution and refinement. Visualization of the crystal structure was carried out with Diamond[33] software.

Powder X-ray Diffraction

For powder X-ray diffraction a phase pure polycrystalline sample was ground thoroughly and sealed in Hilgenberg glass capillaries to avoid hydrolysis. Data was collected on a Stadi-P powder diffractometer (STOE & Cie GmbH, Darmstadt, Germany) equipped with a Mythen 1 K detector (Dectris, Baden, Switzerland) in Debye-Scherrer geometry with Ge(111) monochromator and Cu–Kα1 and

Ag–Kα1 radiation. Rietveld refinement based on single-crystal diffraction data was performed with the TOPAS[34] software.

Solid-State MAS-NMR

Polycrystalline samples of $AE_2Li_4SiP_4$ (AE = Ca, Sr, Eu) were loaded into a commercial zirconia rotor with 2.5 mm in diameter. Spectra of ^{7}Li, ^{29}Si, ^{31}P were acquired on a Bruker Avance III 500 spectrometer device with a magnetic field of 11.74 T. The sample was rotated under MAS conditions with a frequency of 10 kHz and a Larmor frequencies of $\nu_0(^{7}\mathrm{Li}) = 194.41$ MHz, $\nu_0(^{29}\mathrm{Si}) = 99.38$ MHz and $\nu_0(^{31}\mathrm{P}) = 202.48$ MHz.

DFT Calculations

First principle electronic structure calculations were performed based on density functional theory (DFT) and plane wave basis sets with the Vienna ab initio simulation package (VASP).[35–36] The projector augmented waves (PAW)[37] was used with and contributions of correlation and exchange treated in the generalized-gradient approximation (GGA)[38] and the modified Becke-Johnson (mBJ) approach.[39] Structure relaxations using the PBE[38] potential yielded good agreements with the experimental structure. The Brillouin-zones were sampled with 10×8×8 ($AE_2Li_4SiP_4$) and 4×6×2 ($Ba_4Li_{16}Si_3P_{12}$) Γ-centered Monkhorst-Pack k-point meshes. Plane wave energy cutoffs were set to 500 eV and the electronic convergency criterion to 10^{-8} eV. Structure parameters were optimized until interatomic forces were smaller than 10^{-4} eVÅ^{-1}. Phonon band structures were calculated via atomic force constants using the supercell approach implemented in the PHONOPY code.[40–41]

Electrical Conductivity

The samples were ground thoroughly prior to measurement and compacted by uniaxial cold pressing (1000 MPa/2 t) into pellets of about 0.5 to 1 mm thickness and 5 mm diameter. Platinum was sputtered onto the pellets with a Quorum Q150 GB to enhance electrode/sample-contact. No reactions were observed between Pt and the samples. All electrochemical measurements (EIS/CA/CP) were performed using an Ivium compactstat.h and a TSC SW closed impedance cell from rhd instruments kept under argon. EIS and CA were performed in a two-electrode setup, while CP was performed in a pseudo-four-electrode setup. All measurements were conducted at a pressure of 720 kPa. For the impedance measurement, an AC voltage of 100 mV was applied. Impedance measurements were carried out in a temperature range between 25 °C and 75 °C to determine the activation energies using the Arrhenius equation. The impedance spectra were analyzed using the RelaxIS3 software from rhd instruments.

Acknowledgements

We thank Christian Minke for measuring solid-state MAS NMR spectra and Dr. Thomas Bräuniger for discussions. The authors acknowledge the computational resources provided by the Leibniz Supercomputing Centre (www.lrz.de). This work was financially supported by the Deutsche Forschungsgemeinschaft (DFG). Open Access funding enabled and organized by Projekt DEAL.

Conflict of Interests

The authors declare no conflict of interest.

Data Availability Statement

The data that support the findings of this study are available from the corresponding author upon reasonable request.

Keywords: Phosphidosilicates · Lithium · Alkaline earth elements · Crystal structures · Ion conduction

[1] B. Eisenmann, H. Jordan, H. Schäfer, *Mater. Res. Bull.* **1982**, *17*, 95–99. https://doi.org/10.1016/0025-5408(82)90188-X.
[2] L. Toffoletti, H. Kirchhain, J. Landesfeind, W. Klein, L. van Wüllen, H. A. Gasteiger, T. F. Fässler, *Chem. Eur. J.* **2016**, *22*, 17635–17645. https://doi.org/10.1002/chem.201602903.
[3] S. Strangmüller, H. Eickhoff, D. Müller, W. Klein, G. Raudaschl-Sieber, H. Kirchhain, C. Sedlmeier, V. Baran, A. Senyshyn, V. L. Deringer, L. van Wüllen, H. A. Gasteiger, T. F. Fässler, *J. Am. Chem. Soc.* **2019**, *141*, 14200–14209. https://doi.org/10.1021/jacs.9b05301.
[4] H. Eickhoff, L. Toffoletti, W. Klein, G. Raudaschl-Sieber, T. F. Fässler, *Inorg. Chem.* **2017**, *56*, 6688–6694. https://doi.org/10.1021/acs.inorgchem.7b00755.
[5] B. Eisenmann, M. Somer, *Z. Naturforsch. B* **1985**, *40*, 886–890.
[6] B. Eisenmann, J. Klein, M. Somer, *Angew. Chem. Int. Ed. Engl.* **1990**, *29*, 87–88. https://doi.org/10.1002/anie.199000871.
[7] A. Haffner, A.-K. Hatz, C. Hoch, B. V. Lotsch, D. Johrendt, *Eur. J. Inorg. Chem.* **2020**, *617*. https://doi.org/10.1002/ejic.201901083.
[8] B. Eisenmann, J. Klein, *J. Less-Common Met.* **1991**, *175*, 109–117. https://doi.org/10.1016/0022-5088(91)90355–8.
[9] B. Eisenmann, M. Somer, *Z. Naturforsch. B* **1984**, *39*, 736–738. https://doi:10.1515/znb-1984-0607.
[10] J. Mark, J.-A. Dolyniuk, N. Tran, K. Kovnir, *Z. Anorg. Allg. Chem.* **2019**, *645*, 242–247. https://doi.org/10.1002/zaac.201800430.
[11] J. Mark, J. Wang, K. Wu, J. G. Lo, S. Lee, K. Kovnir, *J. Am. Chem. Soc.* **2019**, *141*, 11976–11983. https://doi.org/10.1021/jacs.9b04653.
[12] H. Li, J. Kim, T. L. Groy, M. O'Keeffe, O. M. Yaghi, *J. Am. Chem. Soc.* **2001**, *123*, 4867–4868. https://doi.org/10.1021/ja010413f.
[13] X. Zhang, T. Yu, C. Li, S. Wang, X. Tao, *Z. Anorg. Allg. Chem.* **2015**, *641*, 1545–1549. https://doi.org/10.1002/zaac.201400620.
[14] K. Feng, L. Kang, W. Yin, W. Hao, Z. Lin, J. Yao, Y. Wu, *J. Solid State Chem.* **2013**, *205*, 129–133. https://doi.org/10.1016/j.jssc.2013.07.018.
[15] A. Haffner, T. Bräuniger, D. Johrendt, *Angew. Chem. Int. Ed.* **2016**, *55*, 13585–13588. https://doi.org/10.1002/anie.201607074.
[16] A. Haffner, A.-K. Hatz, O. E. O. Zeman, C. Hoch, B. V. Lotsch, D. Johrendt, *Angew. Chem. Int. Ed.* **2021**, *60*, 13641–13646. https://doi.org/10.1002/anie.202101187.
[17] A. Haffner, A.-K. Hatz, I. Moudrakovski, B. V. Lotsch, D. Johrendt, *Angew. Chem. Int. Ed.* **2018**, *57*, 6155–6160. https://doi.org/10.1002/anie.201801405.
[18] A. Haffner, D. Johrendt, *Z. Anorg. Allg. Chem.* **2017**, *643*, 1717–1720. https://doi.org/10.1002/zaac.201700320.
[19] A. Haffner, V. Weippert, D. Johrendt, *Z. Anorg. Allg. Chem.* **2020**, *646*, 120–124. https://doi.org/10.1002/zaac.201900188.
[20] H. G. von Schnering, G. Menge, *J. Solid State Chem.* **1979**, *28*, 13–19. https://doi.org/10.1016/0022-4596(79)90053–7.
[21] P. Kaiser, W. Jeitschko, *J. Solid State Chem.* **1996**, *124*, 346–352. https://doi.org/10.1006/jssc.1996.0248.
[22] C. Perrier, H. Vincent, P. Chaudouët, B. Chenevier, R. Madar, *Mater. Res. Bull.* **1995**, *30*, 357–364. https://doi.org/10.1016/0025-5408(95)00001–1.
[23] H. Vincent, J. Kreisel, C. Perrier, O. Chaix-Pluchery, P. Chaudouet, R. Madar, F. Genet, G. Lucazeau, *J. Solid State Chem.* **1996**, *124*, 366–373. https://doi.org/10.1006/jssc.1996.0251.
[24] O. Il'nitskaya, V. Bruskov, P. Zavalii, Y. B. KUZ'MA, *Inorg. Mater.* **1991**, *27*, 1108–1110.
[25] P. Kaiser, W. Jeitschko, *Z. Anorg. Allg. Chem.* **1996**, *622*, 53–56. https://doi.org/10.1002/zaac.19966220109.

[26] P. Kaiser, W. Jeitschko, *Z. Naturforsch. B* **1997**, *52*, 462–468. https://doi.org/10.1515/znb-1997-0406.
[27] Y. Mozharivskyj, O. Lang, H. F. Franzen, *Z. Anorg. Allg. Chem.* **2000**, *626*, 2153–2160. https://doi.org/10.1002/1521-3749(200010)626:10<2153::AID-ZAAC2153>3.0.CO;2-X.
[28] J. Wallinda, W. Jeitschko, *J. Solid State Chem.* **1995**, *114*, 476–480. https://doi.org/10.1006/jssc.1995.1071.
[29] G. Sheldrick, *Acta Crystallogr. Sect. A* **2008**, *64*, 112–122. https://doi.org/10.1107/S0108767307043930.
[30] APEX3, Bruker AXS Inc., Madison, Wisconsin, **2016**.
[31] XPREP, Version 2008/2, Bruker AXS Inc., Karlsruhe, Germany, **2008**.
[32] O. V. Dolomanov, L. J. Bourhis, R. J. Gildea, J. A. K. Howard, H. Puschmann, *J. Appl. Crystallogr.* **2009**, *42*, 339–341. https://doi.org/10.1107/S0021889808042726.
[33] K. Brandenburg, Diamond, Version 3.2k, Crystal Impact GbR, Bonn, Germany, **2014**.
[34] A. Coelho, TOPAS-Academic, Version 4.1, Coelho Software, Brisbane, Australia, **2007**.
[35] G. Kresse, J. Hafner, *Phys. Rev. B* **1994**, *49*, 14251–14269.
[36] G. Kresse, J. Furthmüller, *Comput. Mater. Sci.* **1996**, *6*, 15–50. https://doi.org/10.1016/0927-0256(96)00008–0.
[37] P. E. Blöchl, *Phys. Rev. B* **1994**, *50*, 17953–17979.
[38] J. P. Perdew, K. Burke, M. Ernzerhof, *Phys. Rev. Lett.* **1996**, *77*, 3865–3868.
[39] A. D. Becke, E. R. Johnson, *J. Chem. Phys.* **2006**, *124*, 221101. https://doi.org/10.1063/1.2213970.
[40] A. Togo, I. Tanaka, *Scr. Mater.* **2015**, *108*, 1–5. https://doi.org/10.1016/j.scriptamat.2015.07.021.
[41] A. Togo, L. Chaput, I. Tanaka, *Phys. Rev. B* **2015**, *91*, 094306. https://doi.org/10.1103/PhysRevB.91.094306.

Manuscript received: November 7, 2023
Accepted manuscript online: December 26, 2023
Version of record online: January 17, 2024